Effect of wetting layer on electron–hole correlation in quantum discs and rings

2006 J. Phys.: Condens. Matter 18 9493

(http://iopscience.iop.org/0953-8984/18/41/016)

INSTITUTE OF PHYSICS PUBLISHING JOURNAL OF PHYSICS: CONDENSED MATTER

J. Phys.: Condens. Matter **18** (2006) 9493–9507 doi:10.1088/0953-8984/18/41/016

Effect of wetting layer on electron–hole correlation in quantum discs and rings

I D Mikhailov[1], **L F García**[1] **and J H Marín**[2]

[1] Escuela de Física, Universidad Industrial de Santander, AA 678 Bucaramanga, Colombia
[2] Escuela de Física, Universidad Nacional de Colombia, Sede Medellín, AA 3840 Medellín, Colombia

E-mail: mikhail@intercable.net.co

Received 17 June 2006, in final form 11 September 2006
Published 29 September 2006
Online at stacks.iop.org/JPhysCM/18/9493

Abstract

We propose a simple method for calculating the ground state wavefunction of an electron–hole pair confined in a heterostructure formed by a flat quantum dot deposited on a thin wetting layer and imbedded in a matrix made of other material. The calculations of the exciton ground state energy, the electron–hole space pair correlation function and the density of the charge distribution have been performed for $In_{0.55}Al_{0.45}As$–$Al_{0.35}Ga_{0.65}As$ and $Ga_{0.7}Al_{0.3}As$/GaAs quantum discs and rings. It is shown that the increase of the wetting layer thickness and the strength of the external magnetic field applied parallel to the axis lead to a lowering of the inner barrier height reinforcing the tunnelling of the particles into the central hole region. We also analyse the charge distribution related to the spatial separation of the particles due to the difference between masses of the electron and the hole. The variation of the quadrupole momentum sign with the increase of the ring inner radius and the appearance of the dipole momentum oriented in the crystal growth direction with the increase of the wetting layer thickness in the presence of the electron–hole pair are predicted.

1. Introduction

The progress in nanoscale technology has made possible the fabrication of quantum rings (QRs) with a thickness about 2 nm, outer radius between 30 and 70 nm and a well defined centre hole of about 10 nm radius [1]. A strong confinement in the growth direction provides in these structures a considerable penetration of the wavefunctions of both the one-particle and collective states into interior and exterior barrier regions. Therefore the question of whether states of the conduction carriers (electron and hole) and their coupled state (exciton) in this nanostructure could be considered as quasi-one-, two- or three-dimensional is a topic of much interest. Additionally, in the case of a significant difference between electron and hole masses, the degree of their tunnelling in the barrier regions might be very different. Therefore one could expect a considerable spatial separation between particles with different charges in a quantum

ring similarly to a flat $In_{0.55}Al_{0.45}As/Ga_{0.65}Al_{0.35}As$ quantum disc where, as it has been shown earlier in [2], more than 90% of the hole is inside the dot while only about 70% of the electron is inside the dot due to a competition between the confinement and the tunnelling. A richer diversity in the properties of the electron–hole pair in a QR should be expected in comparison with the quantum disc case, owing to the additional possibility of the particles tunnelling in the interior barrier region. The probability for this tunnelling is different for the electron and the hole but in both cases it is significant as a consequence of the small effective barrier height for the particles' in-plane motion. The smaller the height of the QR above the wetting layer (WL) and the greater the thickness of the WL, the lower is the barrier height in the interior junction of the QR for the in-plane motion and the greater is the probability for the tunnelling. Besides, the tunnelling toward the interior barrier region of the QR can be additionally reinforced by introducing an external magnetic field applied parallel to the crystal growth direction. Any accurate theoretical study of this specific character of the magnetoexciton confinement in quantum dots with a ring-like geometry suggests a great computational effort associated to the presence of WLs both in the interior and exterior regions.

Previously, different mathematical techniques such as the finite element [2, 3], variational [4–7], matrix diagonalization [8], or fractional-dimensional [9] methods have been used to analyse the effect of the confinement in quantum dots (QDs) on the exciton spectrum. These techniques give consistent results with the experimental data, but they entail a lot of computational effort. Recently, there has been proposed a simple variational procedure [10] related to the fractal-dimensional approach [11] for calculating the ground state energy of an exciton confined in a heterostructure which provides an efficient algorithm whose accuracy is comparable with that of such sophisticated methods as the series expansion and Monte Carlo technique [10].

In the present work we apply a fractal-dimensional approach in order to calculate the energy, the spatial charge distribution and the electron–hole pair correlation function corresponding to the ground state of an exciton in a QR taking to into account the effects related to the particles tunnelling inside the WL ignored by others authors. We show that the electron–hole pair correlation function can be expressed in terms of the radial part of the wavefunction of a hydrogen-like atom in effective fractional-dimensional space. Our numerical results for the exciton ground state energies in $In_{0.55}Al_{0.45}As/Ga_{0.65}Al_{0.35}As$ and $Ga_{0.7}Al_{0.3}As/GaAs$ quantum discs in the limit case as the WL thickness tends to zero are in a good agreement with those obtained previously by using different methods. It is demonstrated that the spatial charge distribution within and around the ring related to the difference of the effective mass of the electron and the hole is very sensitive to the variation of the outer and centre hole radii, the WL thickness and the magnetic field strength.

2. Model

We describe the geometrical shape of a QR by means of the piecewise constant function $d(\rho)$, which defines the dependence of the thickness d of the In(Al)As layer, embedded in the Ga(Al)As matrix, on the distance ρ from the axis of symmetry. With d_0 the height of the QR above the WL and d_b the thickness of the WL, we assume that $d(\rho)$ is equal to $d_0 + d_b$ inside the QR ($R_{int} < \rho < R_{ext}$), and it is equal to d_b (a few atomic layers) [12] outside the QR (figure 1). Here and in what follows R_{int} and R_{ext} are the interior and exterior radii of the QR.

To be able to make a valid comparison between our method and the full 3D treatment realized in [2] for a quantum disc, we consider for our simulations $In_{0.55}Al_{0.45}As/Al_{0.35}Ga_{0.65}As$ structures with the following values of physical parameters [2]: the dielectric constant $\varepsilon = 12.71$, the effective masses in the dot region and the region outside the dot for the electron are

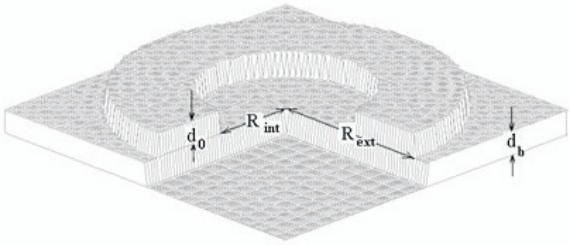

Figure 1. A 3D image of a QR.

$m_{\rm ew} = 0.076\, m_0$ and $m_{\rm eb} = 0.097\, m_0$, respectively, and for the hole $m_{\rm hw} = m_{\rm hb} = 0.45\, m_0$, and the conduction and valence band offsets in the junctions are $V_{0\rm e} = 358$ meV and $V_{0\rm h} = 172$ meV, respectively. Here and in what follows, subscripts e and h correspond to the electron and the hole, respectively. We scale all lengths in terms of the exciton effective Bohr radius $a_0^* = \hbar^2\varepsilon/\mu e^2 \approx 10.4$ nm, all energies are in the exciton effective Rydberg Ry^*, and the magnetic field strength is in terms of the first Landau level energy expressed in Ry^*, $\gamma = e\hbar B/2\mu c Ry^*$, μ being the electron–hole reduced mass inside the dot, $\mu = m_{\rm ew}m_{\rm hw}/(m_{\rm ew} + m_{\rm hw}) \approx 0.065\, m_0$.

With $\mathbf{r}_{\rm e}$ and $\mathbf{r}_{\rm h}$ the electron and hole position vectors, the dimensionless Schrödinger equation for an electron–hole pair in an axially symmetrical QD in the presence of a magnetic field oriented along the z-axis in the effective-mass approximation can be written in cylindrical coordinates ($\mathbf{r}_{\rm p} = \{\rho_{\rm p}, \vartheta_{\rm p}, z_{\rm p}\}$; p = e, h) as

$$\begin{aligned} &H(\mathbf{r}_{\rm e}, \mathbf{r}_{\rm h}, \tau)\Psi(\mathbf{r}_{\rm e}, \mathbf{r}_{\rm h}, \tau) = E(\tau)\Psi(\mathbf{r}_{\rm e}, \mathbf{r}_{\rm h}, \tau);\\ &H(\mathbf{r}_{\rm e}, \mathbf{r}_{\rm h}, \tau) = H_{\rm e}(\mathbf{r}_{\rm e}) + H_{\rm h}(\mathbf{r}_{\rm h}) - 2\tau/r_{\rm eh}; \qquad \tau = 0, 1\\ &H_{\rm p}\left(\mathbf{r}_{\rm p}\right) = -\nabla_{\rm p}\eta_{\rm p}\nabla_{\rm p} + \gamma^2\rho^2/4 + V_{\rm p}\left(\rho_{\rm p}, z_{\rm p}\right); \qquad \eta_{\rm p} = \mu/m_{\rm p}; \qquad {\rm p} = {\rm e, h}. \end{aligned} \tag{1}$$

Here the case ($\tau = 0$) corresponds to the neutral particles and $\tau = 1$ to the electron–hole pair, and $r_{\rm eh}$ denotes the electron–hole separation ($r_{\rm eh} = |\mathbf{r}_{\rm e} - \mathbf{r}_{\rm h}|$). The confinement potential $V_{\rm p}(\rho_{\rm p}, z_{\rm p})$ is equal to zero inside the QR and the WL and it is equal to $V_{\rm op}$, p = e, h outside them. The parameter $\eta_{\rm p}$ for the electron is equal to $\eta_{\rm ew} = 0.86$ in the well and to $\eta_{\rm eb} \approx 0.67$ in the barrier, and for the hole $\eta_{\rm hw} = \eta_{\rm hb} \approx 0.14$.

For the neutral particles $\tau = 0$ the Hamiltonian (1) can be separated, and the energies $E_{m,m'}$ and the functions $\Psi^{(0)}_{m,m'} = \Psi_{m,m'}(\mathbf{r}_{\rm e}, \mathbf{r}_{\rm h}, \tau = 0)$ of two particles with angular momenta $m, m' = 0, \pm1, \pm2, \ldots$ may be found by solving two independent one-particle problems:

$$H_{\rm p} f_{\rm p}^{(m)}\left(\mathbf{r}_{\rm p}\right) = E_{\rm p}^{(m)} f_{\rm p}^{(m)}(\mathbf{r}_{\rm p}); \qquad {\rm p} = {\rm e, h} \tag{2a}$$

$$\Psi^{(0)}_{m,m'} = \Psi_{m,m'}(\mathbf{r}_{\rm e}, \mathbf{r}_{\rm h}, \tau = 0) = f_{\rm e}^{(m)}(\mathbf{r}_{\rm e})\, f_{\rm h}^{(m')}(\mathbf{r}_{\rm h}); \qquad E^{(0)}_{m,m'} = E_{\rm e}^{(m)} + E_{\rm h}^{(m')}. \tag{2b}$$

In order to find solutions of the one-particle wave equations (2*a*) we use the adiabatic approximation [13], in which the rapid motion along z-direction in the cylindrical coordinates can be separated from the slower motions in radial and angular directions and the one-particle wavefunction in a flat QD can be written as

$$f_{\rm p}^{(m)}\left(\mathbf{r}_{\rm p}\right) = {\rm e}^{{\rm i}m\vartheta_{\rm p}} f_{z{\rm p}}\left(z_{\rm p}, \rho_{\rm p}\right) f_{\rho{\rm p}}^{(m)}\left(\rho_{\rm p}\right); \qquad {\rm p} = {\rm e, h}. \tag{2c}$$

Here $f_{z{\rm p}}(z, \rho)$ is the exact ground state wavefunction for one-dimensional motion along the z-axis in a quantum well with the barrier height $V_{0{\rm p}}$ and the well width equal to the thickness $d(\rho)$ of the $In_{0.55}Al_{0.45}As$ layer. The corresponding ground state energy for the motion along the z-direction $E_{z\rho}(\rho)$ depends on the distance from the axis and it is equal to $E_{z{\rm p}}^{(w)}$ inside the

QR ($R_{\rm int} < \rho < R_{\rm ext}$) and to $E_{z{\rm p}}^{(b)}$ outside the QR ($\rho < R_{\rm int}$ or $\rho > R_{\rm ext}$), $E_{z{\rm p}}^{(w)}$ and $E_{z{\rm p}}^{(b)}$ being the lowest level energies in a QW with barrier height $V_{0{\rm p}}$, and well widths d_0 and $d_{\rm b}$, respectively. The radial part of the one-particle wavefunction is the solution of the following two-dimensional central force problem:

$$\begin{aligned} &-\frac{1}{\rho}\frac{\rm d}{{\rm d}\rho}\left[\eta_{\rm p}\rho\frac{{\rm d}f_{\rho{\rm p}}^{(m)}(\rho)}{{\rm d}\rho}\right]+\tilde{V}_{\rm p}^{(m)}(\rho)f_{\rho{\rm p}}^{(m)}(\rho)=E_{\rm p}^{(m)}f_{\rho{\rm p}}^{(m)}(\rho);\\ &\tilde{V}_{\rm p}^{(m)}(\rho)=E_{z\rho}(\rho)+\eta_{\rm p}\left(\frac{m^2}{\rho^2}+\frac{\gamma^2\rho^2}{4}+\gamma m\right). \end{aligned} \tag{3}$$

To find energies $E_{\rm p}^{(m)}$ and the radial parts of the one-particle wavefunctions $f_{\rho{\rm p}}^{(m)}(\rho)$ we solve equation (3) numerically by using the trigonometric sweep method [14].

The two-particle problem (1) for an exciton is not possible to solve exactly and therefore to find the ground state wavefunction $\Psi(\mathbf{r}_{\rm e},\mathbf{r}_{\rm h},\tau=1)$ of the electron–hole pair we employ a variational principle using to this end the Bastard-type trial function in the form of a product of the wavefunction of the neutral particles corresponding to the lowest energy, $\Psi_{m,m'}^{(0)}$, with an unknown variational function, $\Phi(r_{\rm eh})$, which takes into account the particles' correlation caused by electron–hole attraction and depends only on the electron–hole separation:

$$\Psi(\mathbf{r}_{\rm e},\mathbf{r}_{\rm h},\tau=1)=\Phi(r_{\rm eh})\,\Psi_{m,m'}^{(0)}(\mathbf{r}_{\rm e},\mathbf{r}_{\rm h},\tau=0)=\Phi(r_{\rm eh})\,f_{\rm e}^{(m)}(\mathbf{r}_{\rm e})\,f_{\rm h}^{(m')}(\mathbf{r}_{\rm h}). \tag{4}$$

The simple trial function (4) does not take into account the effects related to the mixing of the one-particle states due to the electron–hole attraction. In principle, it could be improved by replacing in (4) the single one-particle wavefunction by a linear combination of functions corresponding to some low-lying states. For the sake of mathematical convenience we use below the simple trial function (4) in which the quantum numbers m and m' refer to the lowest energy levels. In a quantum disc this level is given by $m=m'=0$ in any magnetic field, but in a QR due to the Aharonov–Bohm effect the quantum numbers m and m' increase as the strength of the magnetic field grows.

The energy of the exciton ground state E is found by minimizing the ratio

$$E[\Phi]=\frac{\left\langle f_{\rm e}^{(m)}(\mathbf{r}_{\rm e})\,f_{\rm h}^{(m')}(\mathbf{r}_{\rm h})\,\Phi(\mathbf{r}_{\rm eh})\right|H(\mathbf{r}_{\rm e},\mathbf{r}_{\rm h},\tau=1)\left|f_{\rm e}^{(m)}(\mathbf{r}_{\rm e})\,f_{\rm h}^{(m')}(\mathbf{r}_{\rm h})\,\Phi(r_{\rm eh})\right\rangle}{\left\langle f_{\rm e}^{(m)}(\mathbf{r}_{\rm e})\,f_{\rm h}^{(m')}(\mathbf{r}_{\rm h})\,\Phi(\mathbf{r}_{\rm eh})\right|\left.f_{\rm e}^{(m)}(\mathbf{r}_{\rm e})\,f_{\rm h}^{(m')}(\mathbf{r}_{\rm h})\,\Phi(r_{\rm eh})\right\rangle}.$$

Taking the functional derivative with respect to $\Phi(r)$ gives a wave equation of the form

$$-\frac{1}{P_0(r)}\frac{\rm d}{{\rm d}r}P_1(r)\frac{{\rm d}\Phi(r)}{{\rm d}r}+\frac{2}{r}\Phi(r)=-E_{\rm b}\Phi(r);\qquad E_{\rm b}=E_{\rm e}^{(m)}+E_{\rm h}^{(m')}-E, \tag{5}$$

where $E_{\rm b}$ is the exciton binding energy and the functions $P_0(r)$ and $P_1(r)$ are given by

$$P_0(r)=\int{\rm d}\mathbf{r}_{\rm e}\int\left|f_{\rm e}^{(m)}(\mathbf{r}_{\rm e})\right|^2\left|f_{\rm h}^{(m')}(\mathbf{r}_{\rm h})\right|^2\delta(|\mathbf{r}_{\rm e}-\mathbf{r}_{\rm h}|-r)\,{\rm d}\mathbf{r}_{\rm h} \tag{6}$$

$$P_1(r)=\int{\rm d}\mathbf{r}_{\rm e}\int(\eta_{\rm e}(\mathbf{r}_{\rm h})+\eta_{\rm h}(\mathbf{r}_{\rm h}))\left|f_{\rm e}^{(m)}(\mathbf{r}_{\rm e})\right|^2\left|f_{\rm h}^{(m')}(\mathbf{r}_{\rm h})\right|^2\delta(|\mathbf{r}_{\rm e}-\mathbf{r}_{\rm h}|-r)\,{\rm d}\mathbf{r}_{\rm h}. \tag{7}$$

When the tunnelling of the particles in the matrix region is small the difference between the functions $P_0(r)$ and $P_1(r)$ can be disregarded since the identity $\eta_{\rm e}(\mathbf{r}_{\rm e})+\eta_{\rm h}(\mathbf{r}_{\rm h})=1$ is fulfilled inside the regions of the QR and the WL. In this case $P_1(r)\approx P_0(r)$ and the wave equation (5) acquires a form of that for a hydrogen atom in an effective space with the radial part of the Jacobian $P_0(r)$:

$$-\frac{1}{P_0(r)}\frac{\rm d}{{\rm d}r}P_0(r)\frac{{\rm d}\Phi(r)}{{\rm d}r}+\frac{2}{r}\Phi(r)=-E_{\rm b}\Phi(r) \tag{8}$$

The Jacobian $P_0(r)$ and the envelope function $\Phi(r)$ are intimately related to the spatial pair correlation function (SPCF) $P(r,\tau)$, which gives the density of the probability of finding the electron and hole separated by a distance r:

$$P(r,\tau) = \langle \delta\left(|\mathbf{r}_e - \mathbf{r}_h| - r\right)\rangle = \int \mathrm{d}\mathbf{r}_e \int \delta\left(|\mathbf{r}_e - \mathbf{r}_h| - r\right) |\Psi\left(\mathbf{r}_e, \mathbf{r}_h, \tau\right)|^2 \,\mathrm{d}\mathbf{r}_h. \tag{9}$$

Comparing equations (6) and (9) one can see that the Jacobian is equal to the SPCF for two neutral particles ($\tau = 0$) confined in a nanostructure, $P_0(r) = P(r, \tau = 0)$. For the exciton ($\tau = 1$) the SPCF, $P(r) = P(r, \tau = 1)$, can be presented as

$$P(r) = \int f_e^2\left(\mathbf{r}_e\right) \mathrm{d}\mathbf{r}_e \int \delta\left(|\mathbf{r}_e - \mathbf{r}_h| - r\right) f_h^2\left(\mathbf{r}_h\right) \Phi^2\left(|\mathbf{r}_e - \mathbf{r}_h|\right) \mathrm{d}\mathbf{r}_h = P_0(r)\Phi^2(r) = \chi^2(r). \tag{10}$$

The function $\chi(r) = \sqrt{P(r)} = \Phi(r)\sqrt{P_0(r)}$ can be considered as the one-particle wavefunction associated to the generalized coordinate corresponding to the separation between two particles, whose squared value coincides with the SCPF.

In such a way the function $P_0(r)$ is a measure of the probability to find an electron and a hole separated by the distance r in their free motion in a QD whereas the squared value of the function $\Phi(r)$ gives the ratio of the SPCFs, $\Phi^2(r) = P(r, \tau = 1)/P(r, \tau = 0)$, in their coupled and free states, respectively. Substituting the relation between $\Phi(r)$ and $\chi(r)$ in equation (8) one can obtain the following equation for the two-particle SPCF:

$$-\chi''(r,\tau) + V_{\mathrm{eff}}(r,\tau)\,\chi(r,\tau) = (E - E_e - E_h)\,\chi(r,\tau); \qquad P(r) = \chi^2(r, \tau = 1) \tag{11a}$$

$$V_{\mathrm{eff}}(r,\tau) = -\frac{2\tau}{r} + \frac{\left(\sqrt{P_0(r)}\right)''}{\sqrt{P_0(r)}}. \tag{11b}$$

Once the one-particle wavefunctions of the electron, $f_e(\mathbf{r}_e)$, and the hole, $f_h(\mathbf{r}_h)$, are found, then the effective potential $V_{\mathrm{eff}}(r,\tau)$ (11*b*) can be calculated by using the relation (6) and the one-dimensional wave equation (11*a*) for the SPCF can be solved by using a standard method. One can verify that for the case of the free electron and the hole, as $\tau = 0$ and $E = E_e + E_h$ the solution of equation (11*a*) is $\chi(r, \tau = 0) = \sqrt{P_0(r)}$ and $P(r, \tau = 0) = P_0(r)$.

3. Results and discussion

In our numerical work we find the exciton energy, E, and the SPCF, $P(r)$, from relations (11) by using a trigonometric sweep method [14]. In order to check the accuracy of our numerical procedure, first we have calculated the exciton ground state binding energy in cylindrical GaAs/$Al_{0.3}Ga_{0.7}$As and $In_{0.55}Al_{0.45}As$/$Al_{0.35}Ga_{0.65}$As discs ($R_{\mathrm{int}} = 0, d_b = 0$), and we compare our results with those obtained previously in [5–7] by using the variational method (figure 2(a)) and with the results of the full 3D treatment realized in [2] (figure 2(b)). Besides, we present the comparison of our calculations with the results obtained experimentally in [15] (figure 2(c)). To be able to make a valid comparison, following these references we define the exciton binding energy, E_b, as the difference between the energies of the unbound and bound electron–hole pair:

$$E_b = E(\tau = 0) - E(\tau = 1) = E_e + E_h - E.$$

In figure 2(a), we present the exciton binding energy as a function of the radius of the GaAs/$Al_{0.3}Ga_{0.7}$As disc with a thickness $d_0 = 7$ nm when the WL thickness is equal to zero and we compare our results (solid lines) with variational calculations obtained previously by using

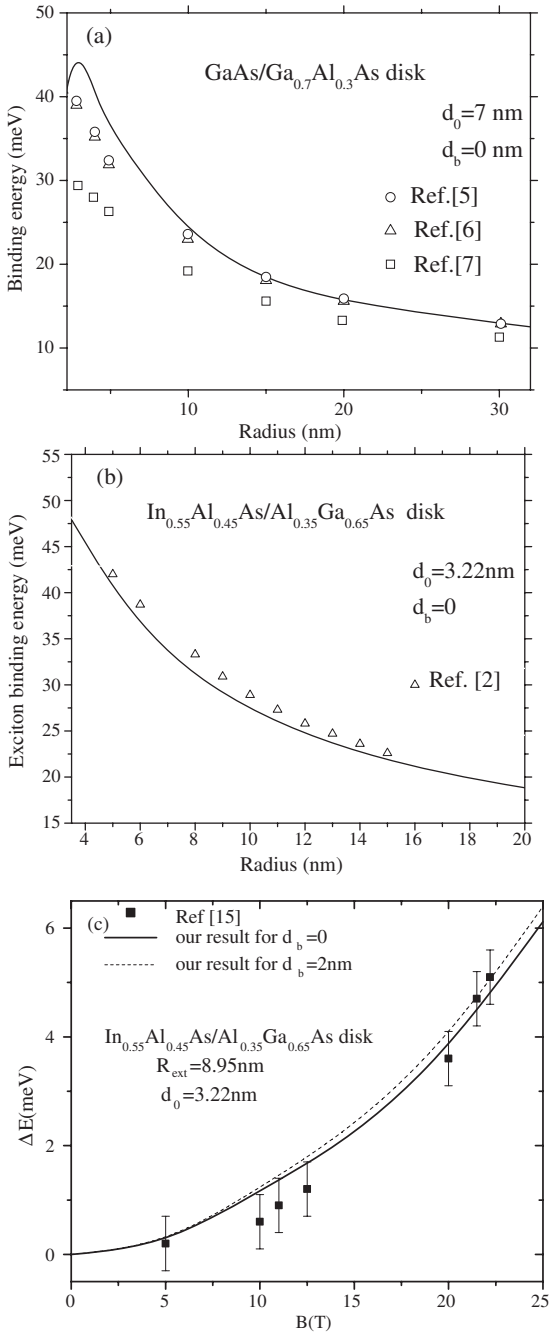

Figure 2. Comparison of our calculations for the exciton ground state binding energy in (a) $GaAs/Al_{0.3}Ga_{0.7}As$ and ((b), (c)) $In_{0.55}Al_{0.45}As/Al_{0.35}Ga_{0.65}As$ structures with theoretical results obtained previously ((a), (b)) and experimentally (c). The discs' parameters are shown in the figures. Our results (solid lines) for exciton ground state binding energies as a function of the quantum disc radius are compared with (a) the variational calculations (different symbols) and (b) full 3D treatment (open triangles). Our calculations (solid and dashed lines) of the diamagnetic shift of the exciton energy as a function of an external magnetic field are compared with the experimental results (squares) in (c).

different types of the trial functions: one-parameter, hydrogen-like (open triangles, [5]), two-parameter (open circles, [6]) and separable (open rectangles, [7]). As the variational calculation gives a lower estimation of the binding energies, the comparison of the results in figure 2(a) shows that for small disc radii our results are better than other variational calculations, whereas for large disc radii our energies are similar to those obtained by using hydrogen-like and two-parameter trial function. This is due to the fact that our trial function which does not use parameters is more flexible in taking into account the change of system symmetry as the disc radius becomes less than one Bohr radius. On the other hand, the comparison of our results with the full 3D treatment presented in figure 2(b) shows that the binding energies obtained by using our procedure are slightly lower than those from [2]; nevertheless, the agreement between the two sets of the energies is excellent, considering the simplicity of our procedure.

Besides, we can compare our calculation with the diamagnetic shift of the exciton ΔE defined as $\Delta E = E(B) - E(B = 0)$ which has been found experimentally in [15]. In figure 2(c) we plotted the exciton diamagnetic shift in $In_{0.55}Al_{0.45}As/Al_{0.35}Ga_{0.65}As$ quantum disc as a function of the magnetic field, where lines indicate our calculated results and squares are the experimental results obtained in [15]. It is seen that the results are in sufficiently good agreement with the experimental results, taking into account the simplicity of our approximate method. It should be noted that our results for a magnetic field stronger 20 T, as should be expected, in contrast to the full 3D treatment realized in [2], start to deviate significantly from the experimental values.

In what follows, we present our results of calculations only for $In_{0.55}Al_{0.45}As/Al_{0.35}Ga_{0.65}As$ nanostructures. Relevant spatial characteristics of the exciton in a QR are the separation between the electron and the hole and the multipole momenta owing to the stronger confinement of the hole in a QD. These characteristics can be expressed in terms of the two-dimensional probability densities of finding of the electron, $\Pi_e(\rho, z)$, and of finding the hole, $\Pi_h(\rho, z)$, at the point with the cylindrical coordinates (ρ, z), which in accordance to the relations (2*c*) and (3) can be calculated as follows:

$$\Pi_e(\rho, z) = \rho f^2_{\rho e}(\rho)\, f^2_{ze}(z, \rho)\, C_h(z, \rho); \qquad \Pi_h(\rho, z) = \rho f^2_{\rho h}(\rho)\, f^2_{zh}(z, \rho)\, C_e(z, \rho); \tag{12a}$$

$$C_p(z, \rho) = \int_0^{\infty} f^2_{\rho p}(\rho_p)\, d\rho_p \int_{-\infty}^{+\infty} f^2_{zp}(z_p, \rho_p)\, dz_p \times \int_0^{2\pi} \Phi^2\left(\sqrt{\rho^2 + \rho_p^2 - 2\rho\rho_p \cos\vartheta + (z - z_p)^2}\right) d\vartheta. \tag{12b}$$

In figure 3 we present the curves of the probability density of finding of the electron, $\Pi_e(\rho, z)$ (solid lines), and the hole, $\Pi_h(\rho, z)$ (dotted lines), given by relations (12) at the points located over the symmetry plane ($z = d_0/2$) as a function of the distance ρ from the axis of two $In_{0.55}Al_{0.45}As/Al_{0.35}Ga_{0.65}As$ QRs with different exterior radii. One can see that in both cases the positive charge predominates in the major part inside the QR, whereas the negative charge predominates outside the QR in the peripheral regions close to the QR junctions. This is due to the fact that the electron effective mass is smaller than that of the hole and therefore the tunnelling of the electron toward both barrier regions (interior and exterior) is larger than the tunnelling of the hole. Also one can observe that the electron tunnelling in the interior barrier region becomes much more significant than that in the exterior region, as the QR interior radius increases. The difference between the electron and hole distributions inside and outside the ring should lead to the predominance of positive charge within the QR and negative charge in the barrier regions close to the junctions.

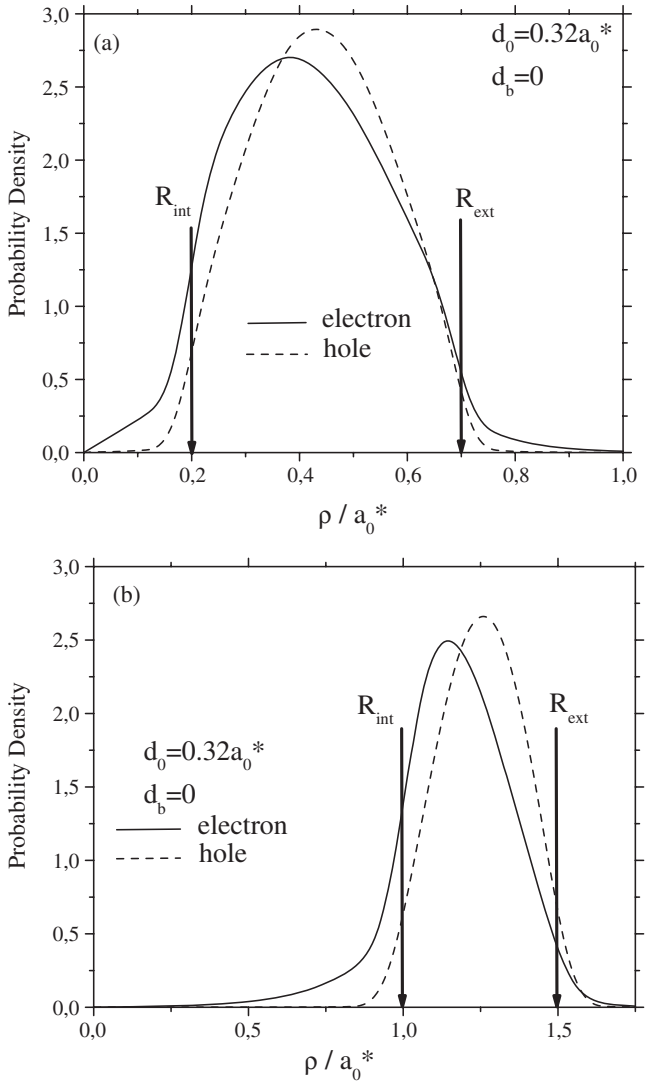

Figure 3. Probability density of finding the electron (solid lines) and the hole (dotted lines) over the symmetry plane as a function of the distance from the axis of QRs with outer radii 0.7 a_0^* (a) and 1.5 a_0^* (b). The width of the QRs in both cases is equal to 0.5 a_0^*. The vertical solid lines show the corresponding QR junction positions.

The corresponding density of charge distribution $Q(\rho, z)$ for an exciton can be calculated as

$$Q(\rho, z) = \Pi_{\mathrm{h}}(\rho, z) - \Pi_{\mathrm{e}}(\rho, z). \tag{12c}$$

In figure 4 we present contour plots, which correspond to the level lines of the exciton charge density of the radial distribution along a cross section in the middle of the quantum discs ((a), (b)) and rings ((c), (d)) perpendicular to the y-direction, calculated by using the relations (12) for structures without ((a), (c)) and with ((b), (d)) a WL. The shadowed parts of the figures indicate the cross section of the corresponding structure parts which become charged positively due to the presence of the exciton.

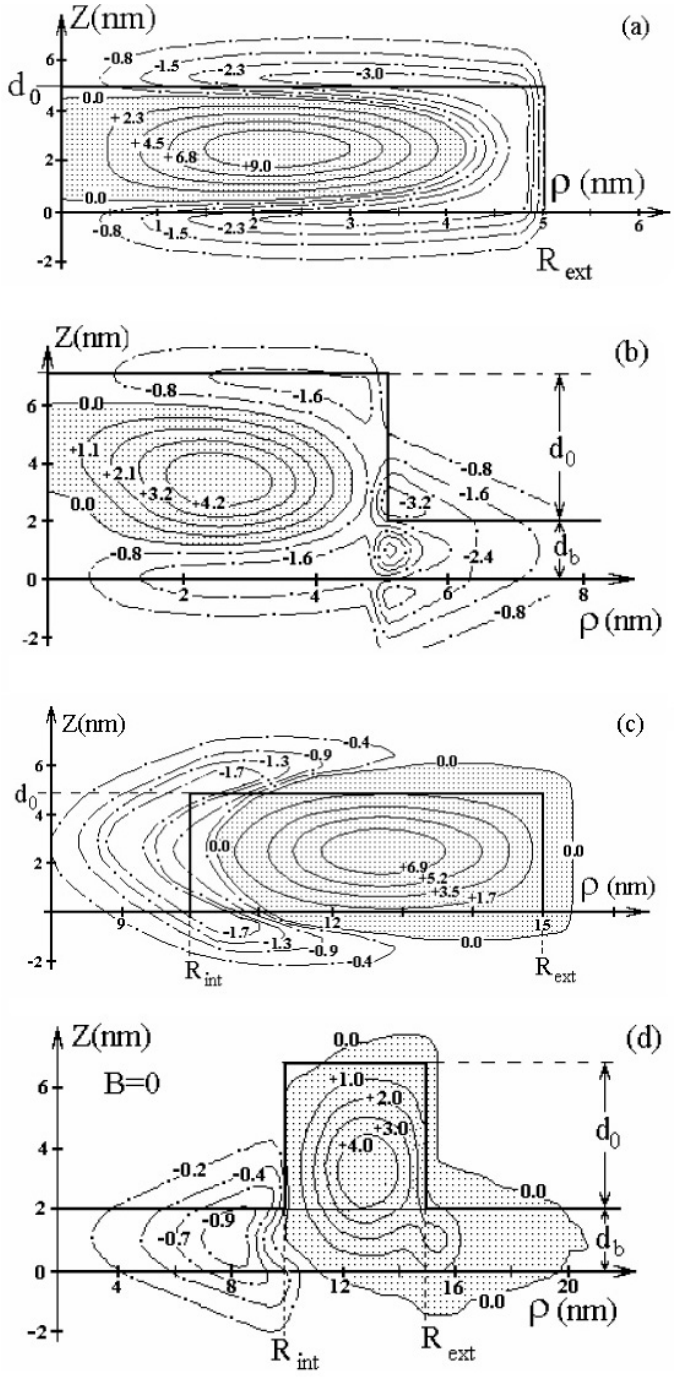

Figure 4. Contour plots of the density of the radial charge distribution in a plane through the axis of symmetry of a quantum disc ((a) and (b)) of radius 5 nm and thickness 5 nm and a QR ((c) and (d)) with interior and exterior radii 10 and 15 nm and thickness 5 nm without ((a) and (c)) and with ((b) and (d)) a wetting layer. Solid lines correspond to positive charge density and dashed–dotted lines are levels with negative charge density.

It is seen from figures 4(a) and (c) that the density of the radial charge distribution inside the disc and ring is positive and it is negative above, below and at the edges of the disc and ring. A similar charge distribution in the presence of an exciton in type-II planar quantum dots has been found previously [16]. Also one can see by comparing figures 4(a) and (c) that if the major part of the negative charge in the quantum disc is located above and below the structure in the quantum ring it is displaced toward the central hole region.

Due to axial symmetry of the structure the dipole moment for both distributions in figures 4(a) and (c) is equal to zero and the charge distribution is characterized by the quadrupole momentum which for the quantum disc in figure 4(a) is positive and for the QR in figure 4(c) is negative. As the thickness of the dot diminishes and it becomes comparable with the of the WL, the electron tunnelling reinforces and the absolute value of the quadrupole momentum increases. It is interesting to analyse the relation of the quadrupole momentum with transformations of the QD morphology. As has been established experimentally [1], the morphology of InAs self-assembled QDs undergoes a remarkable change during the growth process from that of a lens (roughly 20 nm in diameter, 7 nm in height) to one resembling a volcano, with an increased lateral size (between 60 and 140 nm in outer diameter), a reduced height (about 2 nm) and a well-defined centre hole of about 20 nm diameter. In accordance with the results presented in figure 4, the quadrupole momentum has to invert its direction while a lens is transformed to a volcano and its absolute value should be increased significantly due to the drastic reducing of the dot thickness and the increase of the outer radius.

In figures 4(b) and (d) we display similar charge distributions in a quantum disc and a QR whose heights are 5 nm deposited over a WL of 2 nm thickness. The existence of a thick WL provides a significant lowering of the barrier height in lateral junctions, increasing the probability for tunnelling from the QD toward the WL. Therefore the electron tunnelling into the barrier regions, which can be observed in figures 4(a) and (c) for heterostructures without the WL, is transformed into electron leaking inside the exterior WL in the quantum disc in figure 4(b) and into the interior WL of the QR in figures 4(d). As a consequence, in the presence of a thick WL there appears a strong separation between the electron and the hole not only in the radial direction but also in the z-direction, which is characterized by a dipole momentum oriented along the z-axis. It is should be noted that the above results are based on the assumption that the confinement potential is given by a step function in the junctions. As has been shown previously for self-assembled quantum dots of type-II, the strain presented in such structures can significantly change the shape of the confinement potential [17]. Nevertheless, we assume that our results for the charge distribution in quantum discs and rings owing to the exciton trapping are qualitatively acceptable in spite of the fact that our simple model underestimates the strain which is always present in these structures.

The separation between the particles due to stronger electron tunnelling inside the interior WL of a QR may be reinforced or weakened by applying a magnetic field in the direction of the crystal growth. On the one hand, the magnetic field provides an additional confinement displacing both charged particles toward the symmetry axis within the ring, making them closer to each other. On other hand, the energy levels lift, increasing the probability of the tunnelling toward the interior WL, initially only for the lighter electron as the magnetic field is relatively weak and afterwards for the heavier hole as the magnetic field becomes stronger. In the first case the separation between particles increases, whereas in the second case it decreases. Therefore, one can either increase or decrease the exciton binding energy, varying the electron–hole separation by means of the magnetic field.

In figure 5 we display the exciton binding energy dependence on the magnetic field strength in a disc (dashed line) with thickness 5 nm and radius 30 nm, and various QRs with different WL thicknesses, d_b (solid lines). In all cases the thickness, interior and exterior radii of QRs are

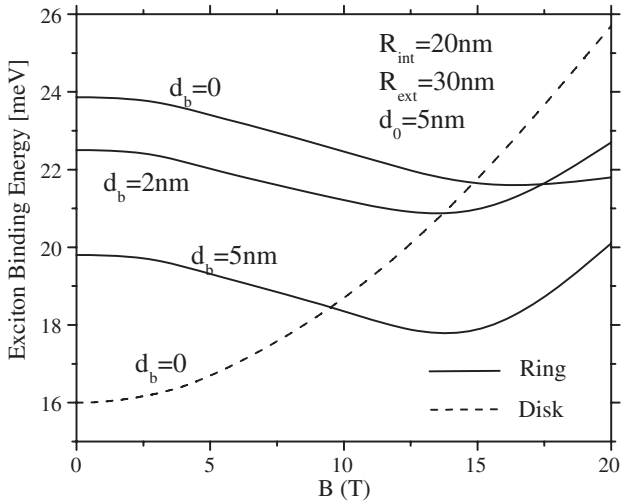

Figure 5. The exciton binding energy as a function of the magnetic field strength in the $In_{0.55}Al_{0.45}As/Al_{0.35}Ga_{0.65}As$ disc (dashed line) and various $In_{0.55}Al_{0.45}As/Al_{0.35}Ga_{0.65}As$ rings with different wetting layer thicknesses (solid lines).

equal to 5, 20 and 30 nm, respectively. As is evident from figure 5, there is a strong correlation between the morphology and the magnetic field dependence of the exciton binding energy. One can see that the exciton binding energy in the disc grows monotonically with increase of the magnetic field which pushes both particles toward the disc axis, making them closer to each other. The morphology of the ring is characterized by the presence of the central hole in the structure and by the existence of two lateral junctions, outer and inner. This is the reason why the curves in figure 5 for QRs are very different. In the ring, as the magnetic field increases, the binding energy first starts to fall until it reaches a minimum. This is due to the fact that under relatively weak magnetic field the heavier particle continues within the ring whereas the lighter one begins to penetrate in the centre hole region and this results in the increasing averaged electron–hole separation. As the magnetic field further increases, the hole also begins to penetrate into the central region and electron–hole separation starts to decrease whereas the binding energy starts to grow. It is seen from figure 5 that the position of the minimum in the curves for the QR depends on the WL thickness. The larger the WL thickness the smaller is the magnetic field strength corresponding to the minimum position. Such dependence of the minimum position is related to the decrease of the barrier height in lateral junctions as the WL thickness grows.

It should be stressed that the magnetic field dependence of the binding energy changes significantly for larger QR thickness, d_0, and smaller thickness of WL, d_b, when there is a significant difference between the electron and the hole probabilities of the tunnelling in the central barrier region as a consequence of an elevated effective lateral barrier height. In figure 6 we present results for QRs with increased thickness, 7 nm, diminished WL height, 1 nm, reduced width, 5 nm, and with different inner radii, 10, 15 and 25 nm. The lateral barrier heights in these structures are significantly more elevated than in case considered above, so that the penetration of the particles inside the central region becomes possible only under a very strong magnetic field.

One can see that the magnetic field dependences in the rings with outer radii 10 and 15 nm are rather similar, and they are very different from the analogous dependence in the ring with

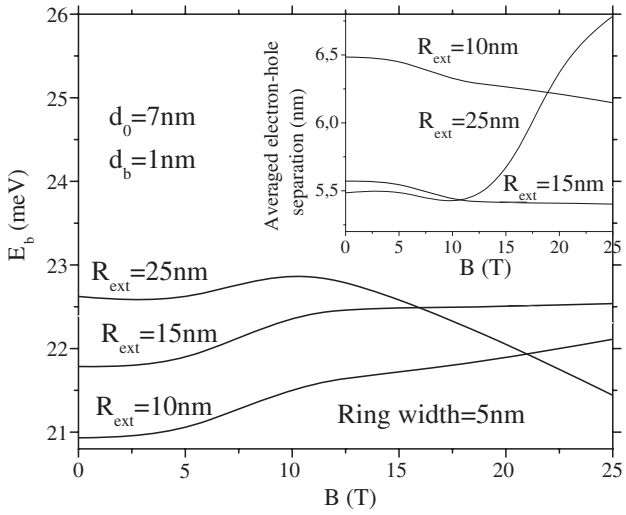

Figure 6. The exciton binding energy as a function of the magnetic field strength in $In_{0.55}Al_{0.45}As/Al_{0.35}Ga_{0.65}As$ rings with different outer radii 10, 15, and 25 nm. In the inset, the averaged electron–hole separation dependence on the magnetic field strength is plotted. The same curve conventions are used as in the main figure.

outer radius 25 nm. If in the first case the binding energy increases monotonically while the magnetic field strength increases to 25 T, the binding energy of the exciton in the QR with outer radius 25 nm first starts to slowly increase until it reaches a maximum for $B = 10$ T and it starts to fall as the magnetic field increases further. In order to facilitate the interpretation of this result we present in the inset of figure 6 the dependence of the averaged electron–hole separation on the magnetic field strength calculated by using to this aim the SPCF given by the relation (10). Comparing the curves in the main figure and in the inset, one can observe a mirror-like similarity of these curves; the smaller the binding energy the larger is the electron–hole separation. It is interesting to note that the averaged electron–hole separation in their bound state in 2D and 3D bulk cases in $In_{0.55}Al_{0.45}As/Al_{0.35}Ga_{0.65}As$ material are equal to half ($\approx$5.2 nm) and one ($\approx$10.4 nm) effective Bohr radius, respectively. Therefore one could interpret the results of calculations for the averaged electron–hole separations presented in the inset as if they were obtained for an exciton embedded in an effective isotropic space whose dimension is fractional and ranged between two and three. This is due to incomplete confinement in the z-direction in any finite thickness structure. Also, it is clear that the increase of the ring radius makes the exciton structure more linear, diminishing additionally the effective dimension of the space. This is a reason why the electron–hole separation in rings with outer radii 15 and 25 nm is appreciably smaller than that in the ring with radius 10 nm. The curvature of the structure in the last case is larger and the exciton configuration is rather two-dimensional than one-dimensional, and conversely in the first case. The height of the effective inner lateral barrier is lowered in the presence of the magnetic field proportionally to the value $\gamma^2 R_{\rm int}^2$. For the considered structures this lowering is insufficient for a significant increasing of the probability of the hole tunnelling in the central region, but it is sufficient for making this probability significant for the electron in a QR with $R_{\rm int} = 20$ nm as the magnetic field strength becomes larger than 10 T. As a result, one can observe in the inset of figure 6 that in these conditions the averaged electron–hole separation starts to increase sharply whereas the binding energy in the main figure starts to fall. Such effect of a drastic increase of the electron–hole

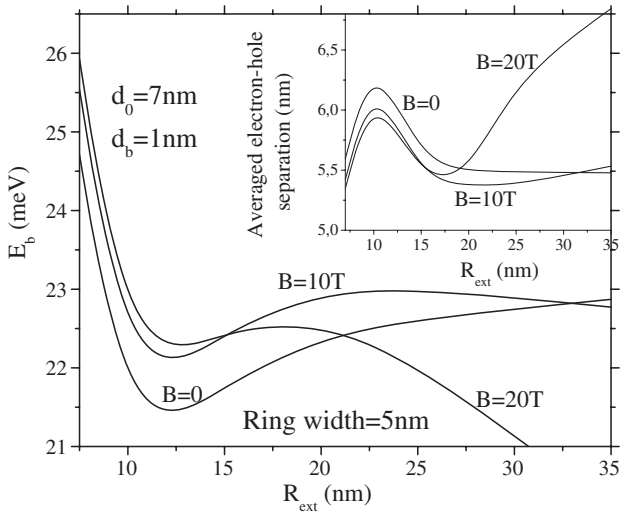

Figure 7. The exciton binding energy as a function of the outer radius in $In_{0.55}Al_{0.45}As/Al_{0.35}Ga_{0.65}As$ QRs with fixed widths for different intensities of the external magnetic field. In the inset, the averaged electron–hole separation dependence on the outer radius is plotted. The same curve conventions are used as in the main figure.

separation and the corresponding decrease of the exciton binding energy can be achieved by applying significantly weaker magnetic field in a QR with larger inner radius that opens some additional possibilities for exciton spectrum handling. As the inner barrier height lowering in the presence of an external magnetic field (proportional to the value $\gamma^2 R_{\mathrm{int}}^2$) depends also on the QR radius, one could expect that the electron–hole separation and the exciton binding energy should be very sensitive to the variation of the QR lateral size. The larger the inner QR radius and the lighter the particle, the higher is the probability for particle tunnelling in the central barrier region. Hence, there is another possibility for a sharp increase of the electron–hole separation by varying the QR radius. In figure 7 we present the results of calculations of the exciton binding energy as a function of the $In_{0.55}Al_{0.45}As/Al_{0.35}Ga_{0.65}As$ outer radius in QRs with fixed width 5 nm for three different values of the magnetic field intensities, 0, 10 and 20 T. In the inset we display the corresponding variation of the averaged electron–hole separation.

It is seen from the inset in figure 7 that as the outer radius, R_{ext}, increases from 7.5 nm (under the condition that the ring width is fixed) the electron and hole first become compressed in the withdrawing opposite sides of the ring and the electron–hole separation increases until it reaches a maximum when R_{ext} becomes equal to approximately one effective Bohr radius (about 10 nm). As R_{ext} further increases, the electron and hole jump on the same side of the ring and the averaged electron–hole separation becomes to decrease rather rapidly. In the presence of a weak or intermediate magnetic field the interior barrier height decreases slowly as the inner radius grows, making possible the electron tunnelling in the central barrier region. As the result the electron–hole separation again starts to increase. One can observe in the inset that such increase is present from $R_{\mathrm{ext}} \approx 17$ nm when $B = 10$ T and from $R_{\mathrm{ext}} \approx 22$ nm when $B = 20$ T. Also one can observe a complete concordance between the curves in the inset and in the main figure. The larger the electron–hole separation the smaller is the exciton binding energy, and vice versa.

4. Conclusions

In order to study the effects of the wetting layer and the external magnetic field on the charge distribution related to the presence of an electron–hole pair in ring-shaped quantum dots we propose a simple method for calculating the ground state wavefunction of an exciton confined in flat quantum discs and rings. We present the multidimensional exciton wavefunction as a product of the one-particle wavefunctions of the electron and the hole (which in our calculations we have found in the adiabatic approximation) with an envelope function that depends only on the electron–hole separation. Starting from the variational principle we show that this function is a solution of the one-dimensional equation which describes the radial part of a hydrogen-like atom in an effective space with a fractional dimension. On the other hand, we have found that the solution of this equation allows us to calculate the electron–hole spatial pair correlation function directly. Our numerical results show that the exciton binding energy, and the averaged electron–hole separation, and related to this the separation charge distribution inside and outside the quantum dot, are very sensitive to the heterostructure morphology, the thickness of the wetting layer and the variation of the magnetic field strength. Such sensitivity of the electronic properties is related to two important factors. The first of them is the lowering of the inner barrier height due to the presence of the wetting layer and the external magnetic field. This lowering reinforces considerably the particles tunnelling inside the central barrier region. The second factor contributing to the particle separations is the considerable difference between the electron and the hole effective masses, making more probable the tunnelling of the electron rather than that of the hole.

We present the results of calculation of the charge distribution in heterostructures with ring-like geometry related to the presence of an exciton. It is found that the peripheral region of the quantum dot is charged negatively and the charged distribution is characterized by a negative quadrupole momentum when the radius of the central barrier region is small. The charge distribution becomes opposite when the radius of the central barrier region becomes sufficiently large. In this case the tunnelling of the electron inside this region predominates, the negative charge is located mainly near the inner junction, and the sign of the quadrupole momentum becomes positive. The situation is also notably changed in heterostructures with an increase of the wetting layer thickness. Our calculations show that in this case the heterostructure acquires a dipole momentum oriented in the crystal growth direction due to the strong electron tunnelling inside the central hole region which becomes charged negatively.

Our simple formalism applied to a simplified model of quantum disc, which ignores the effect of wetting layer, gives results that are in a good agreement with those obtained previously by other authors.

Acknowledgments

This work was financed by the Industrial University of Santander (UIS) through the Dirección General de Investigaciones (DIF Ciencias, Cod. 5124) and the Excellence Centre of Novel Materials—ECNM, under Contract No. 043-2005 and the Cod. No. 1102-05-16923 subscribed with COLCIENCIAS. J H Marín wishes to thank the Universidad Nacional de Colombia, Sede Medellín for permission to study at the UIS.

References

[1] Lorke A, Luyken R J, Govorov A O, Kotthaus J P, García J M and Petroff P M 2000 *Phys. Rev. Lett.* **84** 2223
[2] Janssens K L, Peeters F M and Schweigert V A 2001 *Phys. Rev.* B **63** 205311

[3] Glutsch S, Bechstedt F, Wegscheider W and Schedelbeck F 1997 *Phys. Rev.* B **56** 4108
[4] Kayanuma Y 1991 *Phys. Rev.* B **44** 13085
[5] Goff S L and Stébe B 1993 *Phys. Rev.* B **47** 1383
[6] Koh T S, Feng Y P, Xu X and Spector H N 2001 *J. Phys.: Condens. Matter* **13** 1485
[7] Susa N 1996 *IEEE J. Quantum Electron.* **32** 1760
[8] Garm T 1996 *J. Phys.: Condens. Matter* **8** 5725
Song J and Ulloa S E 2001 *Phys. Rev.* B **63** 125302
Szafran B, Adamowski J and Bednarek S 2002 *J. Phys.: Condens. Matter* **14** 73
Ciurla M, Adamowski J, Szafran B and Bednarek S 2002 *Physica* E **15** 261
[9] He X-F 1990 *Phys. Rev.* B **42** 11751
He X-F 1991 *Phys. Rev.* B **43** 2063
Mathieu H, Lefebvre P and Christol P 1992 *Phys. Rev.* B **46** 4092
Lefebvre P, Christol P and Mathieu H 1993 *Phys. Rev.* B **48** 17308
Reyes-Gómez E, Matos-Abiague A, Perdomo-Leiva C A, Leyva M de Dios and Oliveira L E 2000 *Phys. Rev.* B **61** 13104
[10] Escorcia R A, Robayo R and Mikhailov I D 2002 *Phys. Status Solidi* b **230** 431
Mikhailov I D, Betancur F J, Escorcia R A and Sierra-Ortega J 2002 *Phys. Status Solidi* b **230** 469
Mikhailov I D, Betancur F J, Escorcia R A and Sierra-Ortega J 2003 *Phys. Rev.* B **67** 115317
Mikhailov I D, Betancur F J, Escorcia R A and Sierra-Ortega J 2005 *Physica* B **355** 255
[11] Mandelbrot B B 1982 *The Fractal Geometry of Nature* (San Francisco, CA: Freeman)
[12] Jacaks L, Hawrylak P and Wójs A 1997 *Quantum Dots* (Berlin: Springer)
[13] Palacios J and Hawrylak P 1995 *Phys. Rev.* B **51** 1769
Solomon G S, Trezza J A, Marshall A F and Harris J S Jr 1996 *Phys. Rev. Lett.* **76** 952
Partoens B, Matulis A and Peeters F M 1999 *Phys. Rev.* B **59** 1617
Korkusinski M and Hawrylak P 2001 *Phys. Rev.* B **63** 195311
Mikhailov I D, Marín J H and García F 2005 *Phys. Status Solidi* b **242** 1636
Marín J H, Mikhailov I D and Betancur F J 2006 *J. Phys.: Condens. Matter* **18** 1005
[14] Betancur F J, Mikhailov I D and Oliveira L E 1998 *J. Appl. Phys.* D **31** 3391
[15] Wang P G, Merz J L, Favard S, Leon R, Leonard D, Medeiros-Ribeiro G, Oestreich M, Petroff P M, Uchida K, Miura N, Akiyama H and Sakaki H 1996 *Phys. Rev.* B **53** 16458
[16] Janssens K L, Patroens B and Peeters F M 2001 *Phys. Rev.* B **64** 155324
Janssens K L, Patroens B and Peeters F M 2002 *Phys. Rev.* B **66** 075314
[17] Janssens K L, Patroens B and Peeters F M 2004 *Phys. Rev.* B **69** 235320
Tadic M and Peeters F M 2004 *J. Phys.: Condens. Matter* **16** 8633